Overlap Optimization in Semiconductor Waveguides by Wafer Bonding

Martin Muñoz and Navin B. Patel

***Abstract*—In this work, we show that the use of a wafer-bonding technique, wherein an inverted half-waveguide structure is bonded on the upright half to form a complete waveguide, optimizes the overlap factor present in three-wave parametric interactions realized in $\overline{4}3m$ semiconductor waveguides. These optimized waveguides can be used for efficient frequency-mixing devices which detect or emit infrared light.**

***Index Terms*—Parametric interactions, semiconductor waveguides.**

I. Introduction

NONLINEAR optics allows the creation of new light sources by means of nonlinear wave mixtures known as parametric interactions in a nonlinear medium. Efficient parametric interactions can be obtained when the phase-matching condition (PMC) is satisfied and the nonlinear response of the medium is high. Parametric interactions in waveguides are attractive because the electromagnetic waves involved are confined by considerable distances in a region of order of the wavelength, producing high-efficiency interactions [1]. The $\overline{4}3m$ semiconductor materials are interesting because they have a high nonlinear response characterized by the nonlinear coefficient d_{14}. However, these cubic materials are not birefringent and do not lend themselves to the usual technique of phase matching utilizing the ordinary and extraordinary indices of refraction. Phase matching can be achieved in waveguide structures made of these materials using the modal dispersion properties of different transverse electric (TE) and magnetic (TM) modes [2], [3]. Three-wave mixing in these waveguide structures involves combination of modes like (0,0,0), (1,0,0), (0,1,0), (0,0,1),…,etc., where the digits stand for the order of the modes [3]. Despite achieving the PMC, the efficiency of the mixing process is drastically reduced since the overlap integral $\int f_1(x)f_2(x)f_3(x)dx$ of the three modes across the waveguide is in general extremely small because of the different odd and even spatial profiles of the modes.

In this paper, we propose the use of the wafer-bonding technique to enhance the overlap integral in parametric interactions involving two waves with zero-order modes and one with first order.

In Section II, starting from the wave equations and applying them to a monochromatic field superposition, the generated field amplitude variation, caused by the nonlinear polarization, is obtained. These amplitude expressions clearly show the important role played by the PMC, the overlap integral, and the overlap factor.

Section III shows how the wafer-bonding technique is used to enhance the overlap factor. The fundamentals of this technique are introduced and the features of one structure created with this technique are compared with those of other structure that do not use this technique. Finally, in Section IV, the parametric interaction advantages obtained with the use of the wafer-bonding technique are discussed.

II. Parametric Interactions

The formalism presented here is similar to the one developed by Boyd [3], but there are several important differences. We use the magnetic component of the TM modes instead of its two electric components. Also, in [3], only the case where the mode of higher frequency is TM was considered. Our analysis allows that any one of the modes can be TM. Additionally, we have introduced a definition for the effective nonlinear coefficient d_{eff}, such that the maximum value of the overlap factor is unity, allowing in this way an absolute comparison between the cases involving different mode combinations. Also, the d_{eff} definition allows us to take into account the nonlinear response of the cladding media not considered in [3].

The following development considers waveguides grown in the [100] direction and wave propagation along the [011] direction, as shown in Fig. 1. In this work, we will consider only three media waveguides; however, the ideas presented can be generalized for multilayer waveguides.

The wave equations for the electric and magnetic field with a polarization source $\boldsymbol{P}$ have the following forms [4]:

$$\left[\nabla\times\nabla\times+\frac{1}{c^2}\frac{\partial^2}{\partial t^2}\right]\boldsymbol{E}(\boldsymbol{r},t)=-\mu_0\frac{\partial^2}{\partial t^2}\boldsymbol{P}(\boldsymbol{r},t) \quad (1)$$

$$\left[\nabla\times\nabla\times+\frac{1}{c^2}\frac{\partial^2}{\partial t^2}\right]\boldsymbol{H}(\boldsymbol{r},t)=\frac{\partial}{\partial t}\nabla\times\boldsymbol{P}(\boldsymbol{r},t). \quad (2)$$

Assuming that the field is a superposition of monochromatic fields, (3) and (4) are derived from (1) and (2) for each frequency

$$\left[\nabla^2+\frac{\omega_l^2}{c^2}\varepsilon(\boldsymbol{r},\omega_l)\right]\widehat{\boldsymbol{E}}(\boldsymbol{r},\omega_l)=-\mu_0\omega_l^2\widehat{\boldsymbol{P}}^{(NL)}(\boldsymbol{r},\omega_l) \quad (3)$$

Manuscript received July 10, 2002; revised February 3, 2003.

M. Muñoz is with the Chemistry Department, City College of the City University of New York, New York, NY 10031 USA and also with the Laboratorio de Pesquisa em Dispositivos, Instituto de Física "Gleb Wataghin," Universidade Estadual de Campinas, Unicamp, Campinas 13801-970, SP, Brazil (e-mail: mmunoz@sci.ccny.cuny.edu).

N. B. Patel is with the Laboratorio de Pesquisa em Dispositivos, Instituto de Física "Gleb Wataghin," Universidade Estadual de Campinas, Unicamp, Campinas 13801-970, SP, Brazil.

Digital Object Identifier 10.1109/JQE.2003.810772

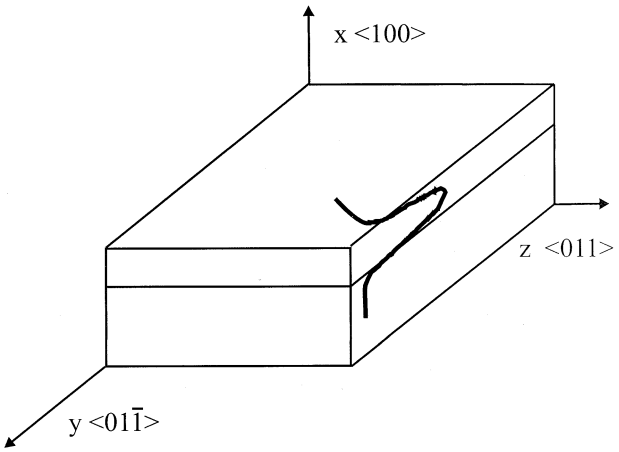

Fig. 1. Waveguide orientation and wave propagation.

$$\left[\nabla^2+\frac{\omega_l^2}{c^2}\varepsilon(\omega_l)\right]\widehat{\boldsymbol{H}}(\boldsymbol{r},\omega_l)=-i\omega_l\left[\varepsilon_0\nabla\varepsilon\times\widehat{\boldsymbol{E}}+\nabla\times\widehat{\boldsymbol{P}}^{(NL)}(\boldsymbol{r},\omega_l)\right] \tag{4}$$

where the notation [4] $\widehat{\boldsymbol{F}}$ refers to the amplitude of the monochromatic oscillation given by $\boldsymbol{F}=1/2\widehat{\boldsymbol{F}}\exp(-i\omega t)+c.c.$ and $\boldsymbol{P}^{(NL)}$ represents the nonlinear component of the polarization $\boldsymbol{P}$.

The nonlinear response of $\bar{4}3m$ semiconductors is characterized by the coefficient d_{14} [4] and by the wave features. For the waveguide of Fig. 1, with the wave propagating in the [011] direction, the nonlinear polarization is given by [3] and in (5), shown at the bottom of the page. According to the last equation, the mode combinations allowed are presented in Table I.

The next development considers the cases 1, 2, and 3 of Table I, which involve only one magnetic field mode.

To estimate the energy exchanged between the waves, we will solve (3) and (4) using the coupled-mode theory [5], in which the energy exchange is due to the coupling caused by some perturbation in the polarization. Following this formalism, we part from a mode superposition of the form

$$\widehat{E}_y=\sum_m a_m(z)\mathcal{E}_y^m(x)e^{-ik_m z} \tag{6}$$

$$\widehat{H}_y=\sum_m a_m(z)\mathcal{H}_y^m(x)e^{-ik_m z} \tag{7}$$

TABLE I
MODE COMBINATIONS FOR PARAMETRIC INTERACTIONS IN $\bar{4}3m$ WAVEGUIDES. TE AND TM REFERS TO THE ELECTRIC AND MAGNETIC MODES, RESPECTIVELY

Case	ω_1	ω_2	$\omega_3=\omega_1\pm\omega_2$
1	TM	TE	TE
2	TE	TM	TE
3	TE	TE	TM
4	TM	TM	TM

where m refers to the order of the TE or TM modes, respectively. Introducing (6) and (7) in (3) and (4), using the slow varying envelope approximation (SVEA) [4] and the orthogonality of the guided modes, it is found that

$$\frac{da_m}{dz}=\frac{e^{ik_m z}}{k_m I_m}\int_{-\infty}^{\infty}r(x)\mathcal{F}_m^* S^{(\omega)}(x,z)dx \tag{8}$$

where

$$r(x)=\begin{cases}1, & \text{if the mode } \mathcal{F}_m \text{ is TE}\\ \frac{1}{n^2(x)}, & \text{if the mode } \mathcal{F}_m \text{ is TM}\end{cases}$$

$$I_m=\int_{-\infty}^{\infty}r(x)\left|\mathcal{F}_m\right|^2dx. \tag{9}$$

Here, $\mathcal{F}_m$ represents the generated field $\mathcal{E}_y^m$ or $\mathcal{H}_y^m$ and $\mathcal{S}^{(\omega)}$ the source $-(i\mu_0\omega^2/2)\hat{\boldsymbol{e}}_y\cdot\boldsymbol{P}_{NL}^{(\omega)}$ or $\omega/2\hat{\boldsymbol{e}}_y\cdot\nabla\times\boldsymbol{P}_{NL}^{(\omega)}$, depending on if the generated field is TE or TM, respectively. The fields $\mathcal{E}_y^m$ and $\mathcal{H}_y^m$ were normalized in accordance to the effective thickness definition used in [6] and [7].

In order to illustrate the importance of the parameters involved, let us consider the frequency sum of two incident waves with modes TM@ω_1 and TE@$\omega_2(\omega_1>\omega_2)$, in this case (8) has the form

$$\frac{de_s}{dz}=i\frac{\omega_s\eta_0^2}{I_s^E}\frac{n_{\text{eff}}^{(1)}}{n_{\text{eff}}^{(s)}}e^{i(k_s-k_1-k_2)z}h_1e_2\cdot\int_{-\infty}^{\infty}d_{14}(x)\mathcal{E}_s^*\frac{\mathcal{H}_1}{n_1^2(x)}\mathcal{E}_2dx. \tag{10}$$

Here, n_{eff} represents the mode effective index, e_2 and h_1 represent the amplitudes of incident electric and magnetic fields with respect to the normalized ones, $\eta_0=\sqrt{\mu_0/\varepsilon_0}$, and $I_s^{\mathcal{E}}$ is given

$$\widehat{\boldsymbol{P}}^{(2)}(\mathbf{r},\omega)=2d_{14}(\mathbf{r},\omega)\begin{pmatrix}-\widehat{E}_y(\mathbf{r},\omega_1)\widehat{E}_y(\mathbf{r},\omega_2)+\widehat{E}_z(\mathbf{r},\omega_1)\widehat{E}_z(\mathbf{r},\omega_2)\\ -\widehat{E}_x(\mathbf{r},\omega_1)\widehat{E}_y(\mathbf{r},\omega_2)-\widehat{E}_x(\mathbf{r},\omega_2)\widehat{E}_y(\mathbf{r},\omega_1)\\ \widehat{E}_x(\mathbf{r},\omega_1)\widehat{E}_z(\mathbf{r},\omega_2)+\widehat{E}_x(\mathbf{r},\omega_2)\widehat{E}_z(\mathbf{r},\omega_1)\end{pmatrix} \tag{5}$$

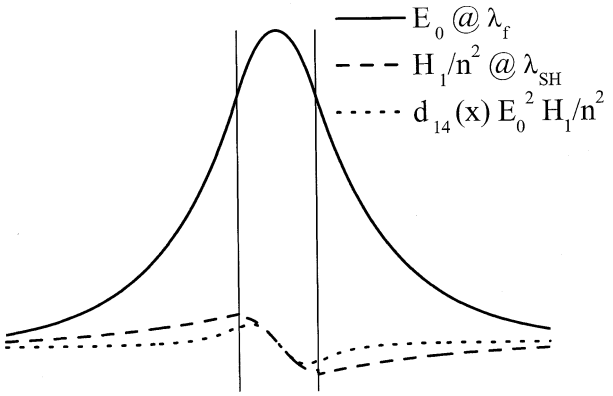

Fig. 2. Fields involved in the SHG and overlap integrand without d_{14} inversion. The vertical lines represent the boundaries of the guiding film.

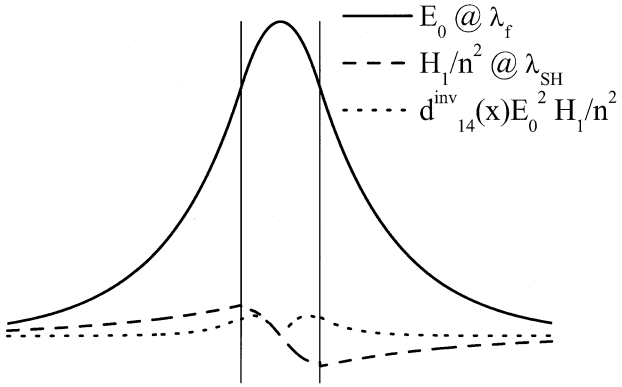

Fig. 3. Fields involved in the SHG and overlap integrand with d_{14} inversion. The vertical lines represent the boundaries of the guiding film.

in (9). The expressions obtained in the others cases from (8) are similar.

The integral that appears in expressions like (10) is known as the *overlap integral* and we will denote it by $I_{\rm ov}$. This integral gives a field-coupling measure weighted by the nonlinear response of the medium.

Under the low efficiency assumption and considering that the field number 3 is generated, it follows that its amplitude can be obtained by direct integration of (8) to give

$$\frac{|f_3|^2}{|f_m|^2} = \Gamma^2 l^2 \operatorname{sinc}^2\left(\frac{\Delta k l}{2}\right)\left(\frac{u_3}{u_1}\right)^2 \tag{11}$$

where

$$\Gamma^2 = \omega_3^2 \eta_0^2 d_{\rm eff}^2 \frac{\left(n_{\rm eff}^{(TM)}\right)^2}{n_{\rm eff}^{(m)} n_{\rm eff}^{(3)}} \delta_m \delta_3 \sigma_3^2 \left|f_M\right|^2 f_{\rm ov}. \tag{12}$$

u_i refers to field units (V/m or A/m), M and m to the incident waves with higher and lower power, respectively, and $f_{\rm ov}$ is the overlap factor defined by

$$f_{\rm ov} = \frac{\frac{1}{d_{\rm eff}^2} I_{\rm ov}^2}{I_m I_3} \tag{13}$$

and

$$\delta_i = \begin{cases} \eta_0, & \text{if } f_i \text{ is TE} \\ \frac{1}{\eta_0}, & \text{if } f_i \text{ is TM} \end{cases} \quad \sigma_i = \begin{cases} 1, & \text{if } f_i \text{ is TE} \\ \frac{(k_i - \Delta k)}{k_i}, & \text{if } f_i \text{ is TM} \end{cases} \tag{14}$$

In (12), we introduced

$$d_{\rm eff} = d_{14}^g r_{\rm TM}^g \tag{15}$$

Where the upper index g means that these quantities correspond to the guiding film.

The $f_{\rm ov}$ definition generalizes the one given in [3], allowing that any one of the wave modes be a TM mode and also take into account the nonlinear response of the cladding media. In the limit case of plane waves this factor reduces to the Boyd one and in consequence its maximum value is unity [3].

III. Overlap Optimization by Wafer Bonding

The wafer-bonding technique [8]–[12] is investigated to integrate GaAs and InP-based devices on Si substrates. Another application of this technique is the crystal axis inversion to obtain quasi-phase-matching [13] in second harmonic generation (SHG) [14].

In this section, we show the use of this technique in optimizing the overlap factor. The idea is illustrated by a SHG example, where a fundamental TE_0 mode generates a harmonic TM_1. In symmetric waveguides epitaxially grown, the product of the fields, illustrated in Fig. 2, involved in the interaction is an odd function, within a symmetric domain, so the overlap integral is zero. However, if only one half of the growth is done and two parts of this are used to bond to each other, the nonlinear coefficient sign of one half will be opposed to the other, as we will prove, as illustrated in Fig. 3. In consequence, the integral of this product now is different from zero, making possible this kind of interaction.

A. Fundamentals

The sign inversion of d_{14} is based in the phase change of the nonlinear polarization by π when one part of the waveguide is oriented in an adequate form. To show the validity of this technique, we will part from the wave equations for the generated fields (3) and (4), and assuming a constant refractive index in each medium, we have

$$\left[\nabla^2 + k_0^2 \varepsilon\right] E_g = -\mu_0 \omega_g^2 \hat{\boldsymbol{e}}_g \cdot \widehat{\boldsymbol{P}}^{NL} \quad \text{TE} \tag{16}$$

$$\left[\nabla^2 + k_0^2 \varepsilon\right] H_g = -i\omega_g \hat{\boldsymbol{e}}_g \cdot \nabla \times \widehat{\boldsymbol{P}}^{NL} \quad \text{TM} \tag{17}$$

where $\hat{\boldsymbol{e}}_g$ refers to the polarization direction of the generated fields, in our case $\hat{\boldsymbol{e}}_g = +\hat{\boldsymbol{e}}_y$.

The inversion of the nonlinear coefficient d_{14} by wafer bonding can be obtained using two configurations. In the first one, the growth is cleaved by the (011) plane, and in the second one by the $(01\overline{1})$ plane, in both cases the bonding is realized by the (100) plane. The first configuration details are shown in Fig. 4, the details for the second configuration are similar.

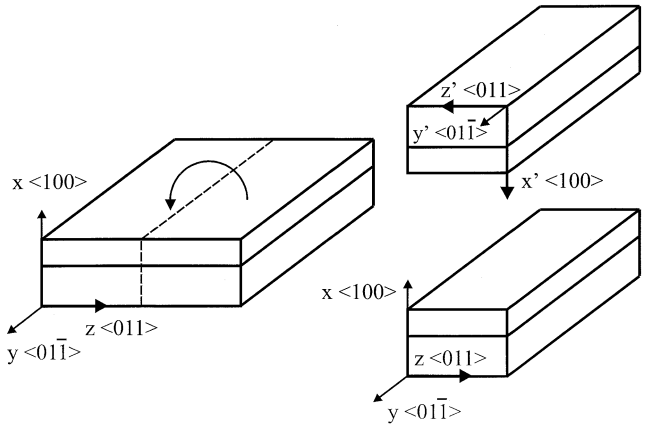

Fig. 4. Details of one configuration used for the overlap enhancement.

According to Fig. 4, the superior axes ($X'Y'Z'$) are related to inferior ones (XYZ) by

$$\hat{e}_g = \hat{\boldsymbol{e}}_{y'} = \hat{\boldsymbol{e}}_y \quad \hat{\boldsymbol{e}}_{x'} = -\hat{\boldsymbol{e}}_x \quad \hat{\boldsymbol{e}}_{z'} = -\hat{\boldsymbol{e}}_z. \tag{18}$$

In this way, the components of the fields propagating along the (011) direction are related by

$$E_{y'} = E_y \quad E_{x'} = -E_x \quad E_{z'} = -E_z. \tag{19}$$

The proof consists of two cases; in the first one, the source is $\hat{\boldsymbol{e}}_g \cdot \widehat{\boldsymbol{P}}^{NL}$ and the generated mode is TE, while in the second one, the source is $\hat{\boldsymbol{e}}_g \cdot \nabla \times \widehat{\boldsymbol{P}}^{\prime NL}$ and the generated mode is TM.

Case 1: The Generated Mode is TE: From (5), the polarization component expressed in the $X'Y'Z'$ axes is given by

$$\hat{\boldsymbol{e}}_g \cdot \widehat{\boldsymbol{P}}^{\prime NL} = 2d_{14}\hat{\boldsymbol{e}}_g \cdot \left[\left(-E_{x'}^{(1)}E_{y'}^{(2)} - E_{x'}^{(2)}E_{y'}^{(1)}\right)\hat{\boldsymbol{e}}_{y'}\right]. \tag{20}$$

Using (18) and (19), we found

$$\begin{aligned}\hat{\boldsymbol{e}}_g \cdot \widehat{\boldsymbol{P}}^{\prime NL} &= -2d_{14}\hat{\boldsymbol{e}}_g \cdot \left[\left(-E_x^{(1)}E_y^{(2)} - E_x^{(2)}E_y^{(1)}\right)\hat{\boldsymbol{e}}_y\right] \\ &= -\hat{\boldsymbol{e}}_g \cdot \widehat{\boldsymbol{P}}^{NL}.\end{aligned} \tag{21}$$

From (20) and (21), it follows that the polarization component is given by

$$\hat{\boldsymbol{e}}_g \cdot \widehat{\boldsymbol{P}}^{NL} = \hat{\boldsymbol{e}}_y \cdot \widehat{\boldsymbol{P}}^{NL} \quad \text{with} \quad \begin{cases} d_{14} > 0, & \text{if } x > 0 \\ d_{14} < 0, & \text{if } x < 0 \end{cases} \tag{22}$$

obtaining in this way the sign inversion of d_{14}.

Case 2: The Generated Mode is TM: In this case $\hat{\boldsymbol{e}}_g \cdot \nabla \times \widehat{\boldsymbol{P}}^{\prime NL} = \partial_{z'}P_{x'} - \partial_{x'}P_{z'}$

From (5), (18), and (19) follows

$$\begin{aligned} P_{z'} &= P_z,\ \partial_{x'} = -\partial_x \Rightarrow \partial_{x'}P_{z'} = -\partial_x P_z \\ P_{x'} &= P_x,\ \partial_{z'} = -\partial_z \Rightarrow \partial_{z'}P_{x'} = -\partial_z P_x \end{aligned} \tag{23}$$

and so

$$\hat{\boldsymbol{e}}'_g \cdot \nabla \times \widehat{\boldsymbol{P}}^{\prime NL} = -\hat{\boldsymbol{e}}_g \cdot \nabla \times \widehat{\boldsymbol{P}}^{NL}. \tag{24}$$

Also, in this case (22) is deduced and the sign inversion of d_{14} is obtained.

For the second configuration, the superior axes ($X'Y'Z'$) are related to inferior ones (XYZ) by

$$\hat{\boldsymbol{e}}_{y'} = -\hat{\boldsymbol{e}}_y = -\hat{\boldsymbol{e}}_g \quad \hat{\boldsymbol{e}}_{x'} = -\hat{\boldsymbol{e}}_x \quad \hat{\boldsymbol{e}}_{z'} = \hat{\boldsymbol{e}}_z. \tag{25}$$

In this way, the field's components are related by

$$E_{y'} = -E_y \quad E_{x'} = -E_x \quad E_{z'} = E_z. \tag{26}$$

The analysis in this case is similar to the first one.

In summary, we have proven that the wafer-bonding technique allows the sign inversion of the nonlinear coefficient d_{14}. This inversion avoids the null overlap factor values for cases involving two zero-order modes and one of first order in a symmetric waveguide.

B. Examples

To determine the significance of the improvements obtained with the wafer-bonding technique, we will compare the values attained by the overlap factor and by the efficiency in two different cases. The compared cases will include one in which the wafer-bonding technique is used and another that only involves zero-order modes, that could be expected to be the best case.

In this comparison, the wafer-bonding technique is applied to an $In_{0.49}Ga_{0.51}P$/GaAs/$In_{0.49}Ga_{0.51}P$ waveguide (W1), and the generation of a zero-order mode is considered in the AlAs-oxide/GaAs/AlAs-oxide waveguide (W2). The incident modes are TE_0 in both cases. In the waveguide W1, the generated wave is a TM_1 mode, and in W2, a TM_0 mode. In the waveguide W2, interactions with all zero-order modes are possible due to the high refractive index step [6].

The refractive indices were taken from [3], [15], [16], the nonlinear coefficients without dispersion from [17], the nonlinear coefficient for the $In_{0.49}Ga_{0.51}P$ was obtained by interpolation of the InP and GaP values, and we considered d_{14} (AlAs-oxide) $= 0$.

The analyzed interaction is the mixture of infrared light (3.2–5 μm with a semiconductor laser $\lambda_s = 1.55$ μm to produce its sum in the Si detector range. The incident power of semiconductor laser is 100 mW and the waveguide length is $l = 1$ mm.

Fig. 5 shows the phase-matching thickness for each infrared wavelength to be detected. For the waveguide W1, there are two possible values for the phase-matching thickness for certain wavelengths around the noncritical point [18] present in $d_{\rm pm} = 0.432$ μm and corresponding to $\lambda_{\rm IR} = 3.23$ μm. In a noncritical point, the thickness variations affect the PMC in a second order.

Fig. 6 presents the uniformity requirements for each thickness shown in the previous graphic. The requirements were evaluated using a Taylor expansion of the phase difference around the phase matching thickness and imposing the condition that the phase change should not be more than π after crossing the waveguide length [3]. This figure shows that the uniformity requirements for the W1 waveguide are less critical than for the W2. Also, the uniformity requirements are relaxed in the neighborhood of the noncritical point. The current epitaxial techniques,

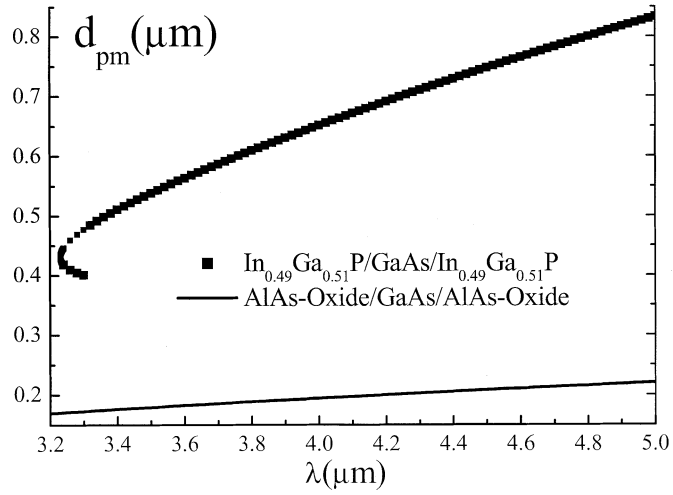

Fig. 5. Phase-matching thickness for $In_{0.49}Ga_{0.51}P/GaAs/In_{0.49}Ga_{0.51}P$ and AlAs-oxide/GaAs/AlAs-oxide waveguides.

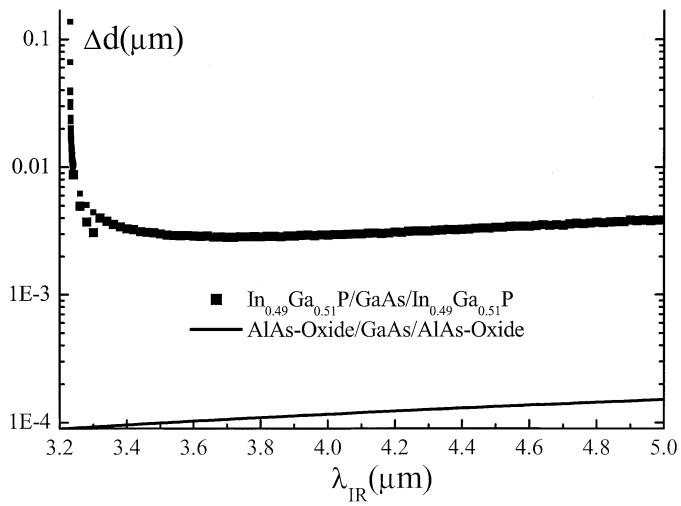

Fig. 6. Uniformity requirements for $In_{0.49}Ga_{0.51}P/GaAs/In_{0.49}Ga_{0.51}P$ and AlAs-oxide/GaAs/AlAs-oxide waveguides.

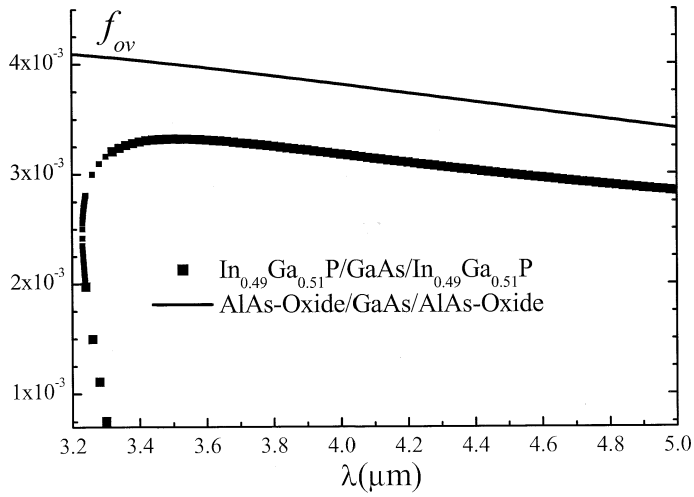

Fig. 7. Overlap factors for $In_{0.49}Ga_{0.51}P/GaAs/In_{0.49}Ga_{0.51}P$ and AlAs-oxide/GaAs/AlAs-oxide waveguides.

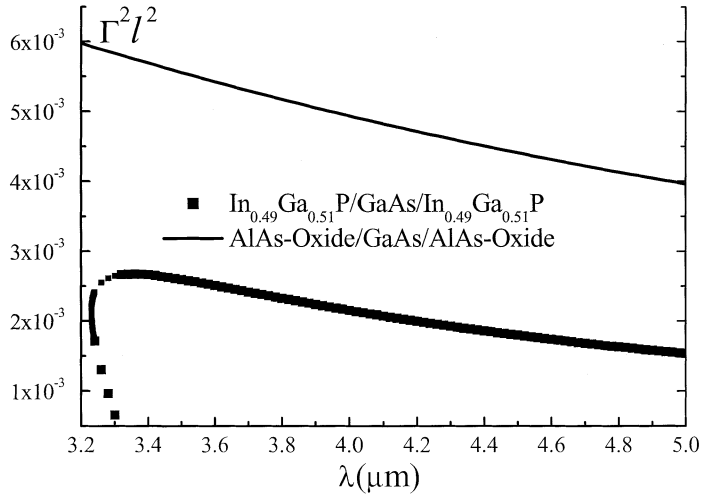

Fig. 8. Efficiency of $In_{0.49}Ga_{0.51}P/GaAs/In_{0.49}Ga_{0.51}P$ and AlAs-oxide/GaAs/AlAs-oxide waveguides.

molecular beam epitaxy (MBE), and metal organic chemical vapor epitaxy (MOCVD), allow the growth of semiconductor monolayers (1–2 Å), which is the fundamental limit for the epitaxial process. Although these techniques offer a great precision of the layer thickness there is a typical variation of 3–5 Å over 1 mm, so it is impossible to construct 1 mm waveguides that require a thickness variation smaller than 3–5 Å. Therefore, Fig. 6 shows that interactions between zero-order modes require waveguides uniformities ranging from a fraction to less than 2 Å, making them unviable.

Fig. 7 shows the overlap values obtained in both interactions. From this, it follows that the overlap values obtained with the wafer-bonding technique are approximately 75% of those obtained in the case that involves zero-order modes only.

Fig. 8 shows that the efficiency of the waveguide created by wafer-bonding is one half of that obtained in the interaction with all modes involved of zero order.

This example shows that the efficiency of the waveguide obtained by the wafer-bonding technique and modes (0,0,1) is a little smaller than the one that only involves zero-order modes. However, the strict uniformity requirements do not allow the construction of this waveguide for the interaction between zero-order modes. For this reason, the overlap optimization technique presented offers an alternative approach to perform parametric interactions in waveguides made of these materials.

IV. Discussion and Conclusions

Two factors determine the efficiency of parametric interactions in waveguides: the PMC and the overlap factor. In order to preserve the PMC, the film uniformity is restricted from fractions of angstroms to a few hundred of them, depending on the waveguide structure. Generally, these uniformity requirements are relaxed when higher order modes are involved. However, high-order modes cause, normally, a drastic diminution in the overlap factor due to the oscillations associated with them [3]. One way to relax the strict uniformity requirements is using noncritical configurations [18], in which the phase matching is affected by thickness variations in second order. The waveguide

InGaP/GaAs/InGaP, presented in our example, is a noncritical configuration for $d_{\rm pm} = 0.432\ \mu$m.

The noncritical configurations are possible only when very strict conditions on both the refractive indices step (ratio) and the thickness of the films are satisfied. For example, in order to realize parametric interactions between zero-order modes, the step of the refractive indices, in a three-medium waveguide, has to be high [18]. In the particular case of SHG, this step has to be at least $\sqrt{2}$ [6], [18], [19].

The relatively small refractive index step (~ 1.2) in the III–V or II–VI semiconductor waveguides only allows phase-matched interactions between zero-order modes if the incident wavelengths are very close or very far from each other. This restriction motivates the consideration of the cases where the order of the two incident waves is zero; meanwhile, the mode of the generated wave can be first or second order. However, this produces a considerable diminution in the overlap factor, therefore it is necessary to use techniques to enhance the overlap factor.

In order to avoid the undesired interference in the overlap factor produced by high-order modes, other techniques [20] introduce linear media in the regions where it is necessary to suppress these effects. However, the use of linear media results in a great part of the incident wave's energy being useless in wave generation. In contrast, the technique that we are proposing uses all the incident energy.

The technique presented in this work gives the possibility of phase matched interactions with two zero-order modes and one first-order mode with a nonzero overlap factor.

The overlap optimization, presented in this work, provides the possibility of the construction of two interesting types of up-converters based on $\overline{4}3m$ semiconductors waveguides. The first one, illustrated in this work, can be used in infrared radiation detection, and the second one, that we plan to explore in the future, is blue-light emission by SHG of a YAG laser in a II–VI semiconductor waveguide.

We have shown that the wafer-bonding technique permits the overlap factor optimization in parametric interactions realized in $\overline{4}3m$ semiconductor waveguides. These waveguides are very promissing due to the semiconductor high nonlinearities and to the growth quality offered by the current epitaxial techniques.

REFERENCES

[1] G. I. Stegeman, "Nonlinear guided wave optics," in *Contemporary Non Linear Optics*, G.P Agrawal and R.W Boyd, Eds. New York: Academic, 1992, pp. 7–40.

[2] P. K. Tien, "Ligth waves in thin films and integrated optics," *Appl. Opt.*, vol. 10, pp. 2395–2413, 1971.

[3] J. T. Boyd, "Theory of parametric oscillation in GaAs thin film waveguides," *IEEE J. Quantum Electron.*, vol. QE-8, pp. 788–796, 1972.

[4] M. Schubert and B. Wilhelmi, "Nonlinear optics and quantum electronics," in *Wiley Series in Pure and Applied Optics*. New York: Wiley, 1986.

[5] A. Yariv, "Coupled mode theory for guided wave optics," *IEEE J. Quantum Electron.*, vol. QE-9, pp. 919–933, 1973.

[6] E. M. Conwell, "Theory of second harmonic generation in optical waveguides," *IEEE J. Quantum Electron.*, vol. QE-9, pp. 867–879, 1973.

[7] H. Kogelnik, "Theory of dielectric waveguides," in *Integrated Optics*, 2nd ed, T. Tamir, Ed. Berlin, Germany: Springer-Verlag, 1979, vol. 7, Topics in Applied Physics, pp. 13–81.

[8] A. Georgakilas, G. Deligeorgis, E. Aperathitis, D. Cengher, Z. Hatzopoulos, M. Alexe, V. Dragoi, U. Gösele, E. D. Kyriakis-Bitzaros, K. Minoglou, and G. Halkias, "Wafer-scale integration of GaAs optoelectronic devices with standard Si," *Appl. Phys. Lett.*, vol. 81, pp. 5099–5101, 2002.

[9] Z. Hatzopoulos, D. Cengher, G. Deligeorgis, M. Androulidaki, E. Aperathitis, G. Halkias, and A. Georgakilas, "Molecular beam epitaxy of GaAs/AlGaAs epitaxial structures for integrated optoelectronic devices on Si using GaAs-Si waferbonding," *J. Cryst.Growth*, vol. 227–228, pp. 193–196, 2001.

[10] H. C. Lin, K. L. Chang, K. C. Hsieh, K. Y. Cheng, and W. H. Wang, "Metallic wafer bonding for the fabrication of long-wavelength vertical-cavity surface-emitting lasers," *J. Appl. Phys.*, vol. 92, pp. 4132–4134, 2002.

[11] Y. H. Lo, R. Bhat, D. M. Hwang, M. A. Koza, and T. P. Lee, "Bonding by atomic rearrangement of InP/InGaAsP 1.5 μm wavelength lasers on GaAs substrates," *Appl. Phys. Lett.*, vol. 58, pp. 1961–1963, 1991.

[12] Y. H. Lo, R. Bhat, D. M. Hwang, C. Chua, and C. H. Lin, "Semiconductor lasers on Si substrates using the technology of bonding atomic rearrangement," *Appl. Phys. Lett.*, vol. 62, pp. 1038–1040, 1993.

[13] J. A. Armstrong, N. Bloembergen, J. Ducuing, and P. S. Pershan, "Interactions between light in a nonlinear dielectric," *Phys. Rev.*, vol. 127, pp. 1918–1939, 1962.

[14] S. J. B. Yoo, R. Bhat, C. Caneau, and M. A. Koza, "Quasi phase matched second harmonic generation in AlGaAs waveguides with periodic domain invertion achieved by wafer bonding," *Appl. Phys. Lett.*, vol. 66, pp. 3410–3412, 1995.

[15] M. H. MacDougal, H. Zhao, P. D. Dapkus, M. Ziari, and W. H. Steier, "Wide bandwidth distributed Bragg reflectors using oxide GaAs multilayers," *Electron. Lett.*, vol. 30, pp. 1147–1149, 1994.

[16] M. Moser, R. Winterhoff, C. Geng, I. Queisser, F. Scholz, and A. Dörnen, "Refractive index of $(Al_xGa_{1-x})_{0.5}In_{0.5}P$ grown by metalorganic vapor phase epitaxy," *Appl. Phys. Lett.*, vol. 64, pp. 235–217, 1994.

[17] O. Madelung, M. Schulz, and H. E. Weiss, *Numerical Data and Functional relationships in Science and Technology Landolt-Börntein*. New York: Springer-Verlag, 1982, vol. LB III 17/a, pp. 185, 218, 281–218, 258, 297.

[18] W. K. Burns and R. A. Andrews, "Non critical phase matching in optical waveguides," *Appl. Phys. Lett.*, vol. 22, pp. 143–145, 1973.

[19] Y. Suematsu *et al.*, "Optical second harmonic generation due to guided wave structure consisting of quartz and glass film," *IEEE J. Quantum Electron.*, vol. QE-10, pp. 222–229, 1974.

[20] H. Ito and H. Inaba, "Efficient phase matched second harmonic generation method in four layered optical waveguide structure," *Opt. Lett.*, vol. 2, pp. 139–141, 1978.

Martin Muñoz was born in Mexico City, Mexico, in 1966. He received the B.Sc. degree in physics and mathematics from the National Polytechnic Institute, IPN, Mexico City, Mexico, in 1988, the M.S. degree from the Center for Research and Advanced Studies, CINVESTAV, Mexico City, Mexico, in 1991, and the Ph.D. degree from the Campinas State University, UNICAMP, Campinas, Brazil, in 1996.

During 1997–1998, he was an Associate Professor in the Physics Department of CINVESTAV. Since 1998, he has been with the City University of New York, where he is presently an Associate Researcher. He has been engaged in the research, growth, and characterization of semiconductor materials and devices since 1994.

Navin B. Patel was born in Tanga, Tanzania, in 1942. He received the B.Sc. degree in physics from the University of Bombay, Bombay, India, in 1963, and the M.S. and Ph.D. degrees in physics from the California Institute of Technology, Pasadena, CA, in 1967 and 1971, respectively.

In 1971, he joined the Universidade Estadual de Campinas (UNICAMP), Campinas, Brazil, where he was a Professor with the Department of Applied Physics until 1995, when he retired from academic life.